# Altered cortico-cerebellar connectivity in cerebellar degeneration patients improves with motor training

**Caroline Nettekoven[1*,2], Rossitza Draganova[3,4], Katharina M Steiner[3,5,6], Sophia L Goericke[7,8], Andreas Deistung[9,10], Jürgen Konczak[11,12], and Dagmar Timmann[3,13]**

[1]**Western Institute for Neuroscience, Western University, London, Ontario, Canada**
[3]**Department of Neurology and Center for Translational Neuro- and Behavioral Sciences (C-TNBS), University Hospital Essen, University of Duisburg-Essen, Essen, Germany**
[5]**LVR-University-Hospital Essen, Department of Psychiatry and Psychotherapy, Medical Faculty, University of Duisburg-Essen, Essen, Germany**
[7]**Institute of Diagnostic and Interventional Neuroradiology and Radiology and C-TNCS, University Hospital Essen, University of Duisburg-Essen, Essen, Germany**
[9]**Department for Radiation Medicine, University Clinic and Outpatient Clinic for Radiology, University Hospital Halle (Saale), Halle (Saale), Germany**
[11]**School of Kinesiology, University of Minnesota, Minneapolis, Minnesota, USA**
[2]`orcid.org/0000-0001-5427-2907`
[4]`orcid.org/0000-0003-0334-2981`
[6]`orcid.org/0000-0002-2181-4295`
[8]`orcid.org/0000-0003-1552-4475`
[10]`orcid.org/0000-0002-2427-1302`
[12]`orcid.org/0000-0002-4422-5610`
[13]`orcid.org/0000-0003-1935-416X`

## ABSTRACT

People with cerebellar degeneration show characteristic ataxic motor impairments. In the early stages of degeneration they can still improve motor function with sensorimotor training. Yet, how such training affects functional brain networks affected by cerebellar degeneration is unknown. We here investigated neuroplastic changes in the cortico-cerebellar network after a five-day forearm movement training in 40 patients with mild to severe cerebellar degeneration and 40 age- and sex-matched healthy controls. Participants were assigned to one of four motor training conditions, varying online visual feedback and explicit verbal feedback. Anatomical and resting-state fMRI was collected on the days before and after training. To overcome the limitations of standard brain templates that fail in the presence of severe anatomical abnormalities, we developed a specific template for comparing cerebellar patients with age-matched controls. Our new template reduced the spatial spread of cerebellar anatomical landmarks by 30% relative to existing templates and tripled fMRI noise classification accuracy. Using this pipeline, we found that patients showed impaired connectivity between cerebellar motor regions and neocortical visuomotor and premotor regions at baseline compared to controls, whereas their cortico-cortico connectivity remained intact. Training with vision strengthened connectivity in the cortico-cerebellar visuomotor network contralateral to the trained arm in all participants. Cerebellar patients exhibited additional increased connectivity ipsilateral to the training arm in this network. Further, training with explicit verbal feedback facilitated connectivity between a cerebellar cognitive region and dorsolateral prefrontal cortex. These results indicate that motor training in cerebellar degeneration leads to enhanced functional connectivity of the cortico-cerebellar network.

Keywords: Cerebellum, Neurodegeneration, Functional connectivity, Motor training, Spinocerebellar ataxia, Resting-state fMRI

# 1 INTRODUCTION

Dysfunction of the cerebellum causes deficits in the coordination and control of gait, posture, speech and fine motor movements. While the recovery of motor function after acute lesions of the cerebellum such as stroke typically happens within weeks and is often complete [1], cerebellar neurodegeneration occurs over years and the ataxic motor symptoms worsen over time. For those affected by cerebellar degeneration, no medication has been proven effective and potential gene therapies are still in the early stages of development [2, 3, 4]. Existing therapies in patients with cerebellar degeneration therefore focus on mitigating symptoms through physical rehabilitation [5, 4]. Continuous and intensive motor training has been shown to improve motor function in cerebellar patients [6, 7, 8, 9, 10]. However, no consensus exists on which type of training is most beneficial for cerebellar patients [4]. Understanding the neuroplastic changes that result from diverse types of motor training could help aid the development of tailored rehabilitation strategies for cerebellar patients.

Motor learning is considered an implicit learning process that relies on processing movement-relevant information from multiple sensory modalities such as vision and proprioception. It relies on an intact network comprising the cerebellum, the basal ganglia, sensorimotor cortex to modulate spinal or brain stem motor neurons. Given that the cerebellum is essential for motor learning and cerebellar degeneration impairs such learning, the utility of movement training programs has been questioned [11, 12, 13]. Indeed, empirical evidence shows that the ability to adapt to external forces, a form of implicit motor learning, can become abolished in the severe stages of cerebellar degeneration [14]. However, recognizing the degenerative process typically spans over years, motor training has also been shown to improve motor function in cerebellar patients who exhibit mild to moderate stages of cerebellar degeneration [6, 7, 8, 9, 10]. The extent of learning on a force adaptation task, has been found to correlate with the severity of ataxia in cerebellar patients with the most severely affected patients showing the smallest amount of learning [14]. To date, no physical rehabilitation programs exist that take the amount of residual sensorimotor function present in the patient into account.

It is well established that proprioceptive afferent signals are vital for motor learning and that the cerebellum receives large proprioceptive afferents through the spinocerebellar tracts [15]. In this context, it is noteworthy that proprioceptive perception is largely intact in people with cerebellar dysfunction as studies reported unimpaired limb position sense when the limb is passively rotated and no voluntary muscle activation is required [16, 14]. However, cerebellar patients show impaired active position sense that relies on voluntary movement [16]. A training protocol that focuses on proprioceptive cues could potentially drive learning in cerebellar patients, but the extent to which patients can use proprioceptive information remains elusive.

Explicit error feedback given by a teacher, for example, can aid motor learning. This indicates that additional cognitive processes involving additional networks occur in parallel and can contribute to motor learning outcomes [17, 18]. Research showed that cerebellar patients rely on explicit re-aiming strategies to counter rotations in a visuomotor adaptation task [19], which implies that they may benefit from additional explicit feedback during motor training.

Animal work suggests that training can slow down the process of degeneration [20, 21]. For people with cerebellar degeneration, motor training over several days led to structural changes in the neocortex, specifically grey matter increase in the premotor cortex [6, 22]. Documenting changes in functional and structural connectivity can provide an additional, more detailed description of the initial impairment and associated training-related changes of the sensorimotor network. Functional activity and connectivity alterations have repeatedly been found in cerebellar patients [23, 24, 25, 26, 27]. Functional connectivity measured by resting-state fMRI has been shown to reliably dissociate patients from controls at 92% accuracy [28]. Functional connectivity changes might therefore hold potential for monitoring disease progression in response to putative therapeutic interventions.

However, a major obstacle to capturing connectivity changes in people with cerebellar degeneration are inadequate neuroimaging analysis pipelines. Normalizing degenerating brain structures to brain templates that are developed on neurologically healthy brains is challenging [29, 30, 31, 32], which limits our ability to detect patient-control differences at the group level. This is compounded by difficulties in aligning cerebellar structures [33], low sensitivity of MRI acquisition coils to cerebellar signal [34], and high noise levels induced by cardiac and respiratory cycles in areas close to the brain stem [35]. Hence, tailoring analysis pipelines to preserve cerebellar signal, particularly in patient populations, is crucial to revealing meaningful changes in connectivity.

In this study, we investigated the neuroplastic changes in cortico-cerebellar connectivity in a sample of patients with cerebellar degeneration induced by extensive motor training of their dominant right arm. The relevant behavioral and structural data have been published in Draganova et al., 2022 [22]. The results showed that participants improved performance during visuomotor practice accompanied by increase grey matter in premotor cortex, but a training focusing on either proprioceptive feedback, or explicit verbal feedback and instruction did not yield additional benefits. We developed a neuroimaging pipeline that substantially improved spatial localization by building a specialized template for comparing cerebellar patient data to data from healthy controls. Using this pipeline, we analyzed the functional connectivity in this dataset and reveal robust and specific cortico-cerebellar connectivity changes that depend on the type of motor training.

# 2 RESULTS

To understand the effect of different types of training on resting-state functional connectivity, we developed a 5-day training protocol with varying task demands (see 4.2). During training, 40 patients with cerebellar degeneration and 40 age-and sex-matched healthy controls performed elbow flexion movements in the horizontal plane with their right arm using a one degree of freedom single-joint manipulandum (described in [36]; Figure 1A). All participants were right-handed as assessed by the Edinburgh handedness scale [37] and performed the task with their right arm. Participants were assigned pseudo-randomly to one of four training conditions, varying the type of feedback provided during and after the movement. During the movement, vision was either occluded through a mask (No Vision) or visual feedback was provided through a laser attached to the manipulandum (Vision). After the movement, the experimenter either provided explicit verbal feedback about the final position in relation to the target and how the target aim can be improved (Explicit Feedback) or no verbal feedback was provided (No Explicit Feedback). To quantify neural changes driven by training, structural and functional resting-state MRI data was acquired on the days before (pre) and after (post) the 5-day training (Figure 1B). Behavioral and structural data have been reported in Draganova et al., 2022 [22].

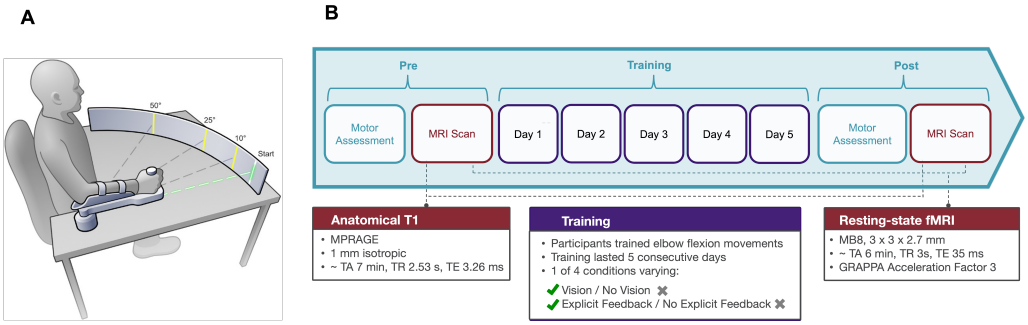


**Figure 1.** Study Design and Motor Training. **A** Experimental setup of the single-joint manipulandum used for motor training. Start position was at 90°elbow flexion. A low-intensity laser attached to the manipulandum provided visual feedback of arm position online. An optical encoder embedded in the housing recorded forearm position. Figure reproduced from Draganova et al., 2022. **B** Participants participated in a five-day training with MRI sessions before (pre) and after training (post). Anatomical T1-weighted and resting-state fMRI data was collected during pre and post MRI sessions.

## 2.1 Study-specific template improves spatial overlap

Anatomical abnormalities present in older adults and brains with cerebellar degeneration [38, 39, 30, 40, 41, 42, 43, 44], pose a challenge for accurate registrations to standard brain templates which are based on young, healthy adults. To improve spatial registration we therefore developed the **De**generation**Con**trol (DeCon) template, a template derived from the brains of cerebellar degeneration patients and controls in our study (Fig. 2A, see 4.4.1). We used 40 anatomical scans, balanced across groups, timepoints and conditions (see Supplementary Table 1).

To validate the use of the DeCon template, we examined the spatial overlap of anatomical landmarks after registration to the DeCon template (see 4.4.1). We compared this to the spatial overlap after

registration to two standard templates used widely in neuroimaging analysis of the cerebellum which are based on young, healthy brains: the MNI template [45] and the SUIT template [33]. To ensure that our comparison is not biased towards the DeCon template, as it represents the average anatomy of those specific individuals, we repeated our analysis with anatomical scans from the 40 independent participants that were not used for template generation (validation sample).

Two major cerebellar fissures, the primary and intrabiventer fissure were drawn on the native structural scan of each individual and transformed into DeCon, MNI and SUIT space. To quantify fissure overlap, we calculated the average fissure distances between all possible pairs of participants. The primary and intrabiventer fissures showed a 30% higher overlap in DeCon space than in both MNI and SUIT space (Fig. 2A). The largest reduction of fissure distances was found in the vermal portion of the primary fissure (see Supplementary Table 2). The primary fissure in the vermal portion was $\tilde{0}.9$ mm apart in the DeCon template, compared to 2-3 mm in MNI and SUIT space (Fig. 2D). Paired t-tests demonstrated that the 70% reduction in fissure distances from MNI space and 60% reduction from SUIT space were significant for both the template generation sample (DeCon vs. MNI: $t_{39} = -15.49, p = 2.97 \times 10^{-18}$; DeCon vs. SUIT: $t_{39} = -13.68, p = 1.82 \times 10^{-16}$) and the independent test sample (DeCon vs. MNI: $t_{39} = -12.9, p = 1.18 \times 10^{-15}$; DeCon vs. SUIT: $t_{39} = -7.88, p = 1.36 \times 10^{-09}$). We next tested for a difference in alignment within the whole cerebellar volume. In the whole cerebellum, we found a smaller, but substantial decrease of 40% for MNI and 30% for SUIT space in primary fissure distance in the template sample (DeCon vs. MNI: $t_{39} = -14.91, p = 1.06 \times 10^{-17}$; DeCon vs. SUIT: $t_{39} = -13.43, p = 3.28 \times 10^{-16}$) and the validation sample (DeCon vs. MNI: $t_{39} = -15.67, p = 2.02 \times 10^{-18}$; DeCon vs. SUIT: $t_{39} = -11.32, p = 6.83 \times 10^{-14}$; Fig. 2B). This echoes observations from Schmahmann et al., 2000[46], who noted that vermal sections of the primary fissure and other fissures are much more pronounced than hemispheric sections, resulting in blurrier fissure boundaries in cerebellar templates as the fissure extends more laterally [33]. In line with this, the DeCon template achieved a 40% and 30% reduction for intrabiventer fissure distance from the MNI template and the SUIT template, respectively (Generation sample, DeCon vs. MNI: $t_{39} = -13.05, p = 8.20 \times 10^{-16}$; DeCon vs. SUIT: $t_{39} = -10.11, p = 1.90 \times 10^{-12}$; Validation sample, DeCon vs. MNI: $t_{39} = -18.46, p = 7.08 \times 10^{-21}$; DeCon vs. SUIT: $t_{39} = -15.1, p = 6.95 \times 10^{-18}$).

To ensure that no systematic differences were present in anatomical alignment due to pathological anatomy, we tested for differences in fissure overlap between patients and controls in DeCon space using independent sample t-tests. We found no significant patient-control differences for the vermal primary fissure ($t_{78} = 1.05, p = 0.30$), the primary fissure across the whole cerebellum ($t_{78} = 1.09, p = 0.28$) or the intrabiventer fissures across the whole cerebellum ($t_{78} = 1.61, p = 0.11$). Our results demonstrate that the DeCon template substantially improves anatomical alignment in the cerebellum compared to existing templates, without favouring the anatomy of healthy control participants.

Finally, we asked whether the improvement in anatomical alignment results in better localization of functional data. For this, we used the automated classifier FIX [47] to identify noise in the resting-state time series data (see 4.4.2). Among several features used for noise classification, FIX uses masks of the major draining veins to identify features of vein-driven noise [47]. Because these masks are drawn in MNI-space and resampled to functional space, FIX's ability to detect noise relies in part on an accurate mapping between MNI space and native functional space. We provided FIX with mappings between functional and MNI space estimated via the subject's anatomical image only, or via the DeCon template 4.4.1 as an intermediate step between anatomical image and the MNI template. We then compared leave-one-out classification accuracy of FIX trained on hand-labelled signal and noise components across a range of classification thresholds in terms of correctly identified noise (true noise rate) and a weighted average between true noise rate and true signal rate (see 4.4.2). Since FIX requires whole-brain registration, we only compared performance with the DeCon template, a whole-brain template. We did use the SUIT template as a comparison, since SUIT provides only a cerebellum template. Across classification thresholds, alignment via the DeCon template resulted in 46% more true noise components detected than alignment directly to MNI space (Paired t-test of true noise rate for DeCon vs. MNI $t_{40} = 10.51, p = 4.54 \times 10^{-13}$; Fig. 2E). Thus, the improved anatomical alignment to MNI space using the DeCon template yields higher accuracy in localizing functional data and hence, better noise feature detection. Finally, to remove structured noise from the resting-state data, we applied FIX-cleaning at threshold 30, where the weighted ratio of classification accuracy was highest (Fig. 2E).

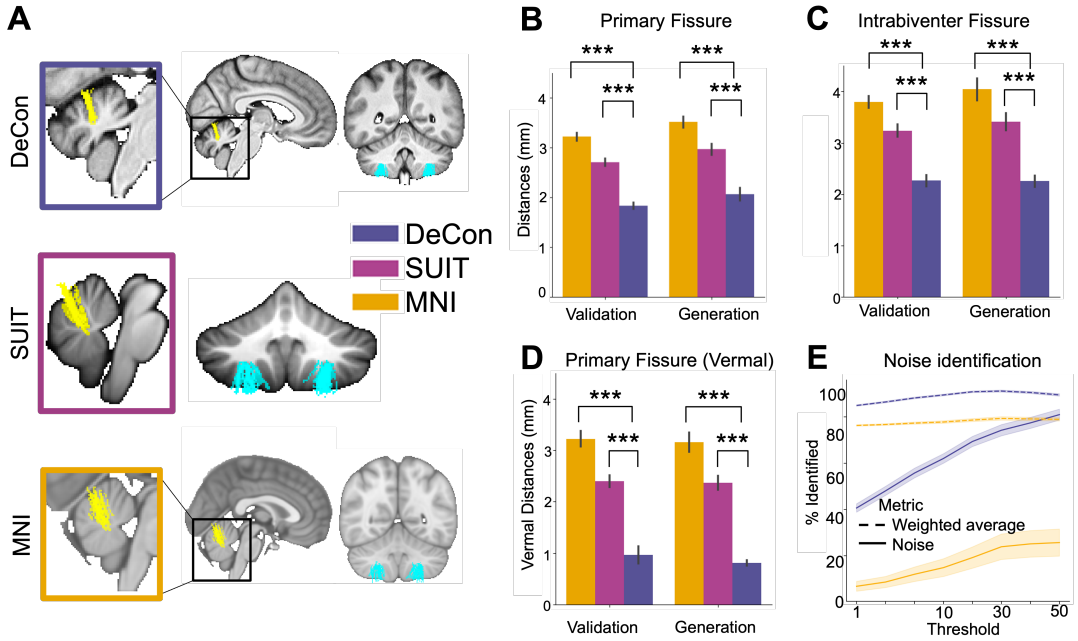


**Figure 2.** DeCon template improves anatomical alignment and functional localization. **A.** Primary (yellow) and intrabiventer (turquoise) fissures registered to the MNI, SUIT and DeCon template show the highest spatial overlap in DeCon space. Only fissures of participants that were not used for template generation are shown (n=40). **B-C.** Fissure overlap, computed as the average fissure distances between all possible pairs of participants, in MNI space (orange), SUIT space (magenta) and DeCon space (blue) is lowest in DeCon space. **B.** Primary fissure distance calculated within the whole cerebellum. **C.** Intrabiventer fissure distance calculated within the whole cerebellum. **D.** Primary fissure distance calculated within vermis. **E.** Percentage of correctly identified noise (solid line) and weighted ratio of correctly identified noise and signal (dashed line) when registering to the MNI template directly (orange) or via the DeCon template (blue). *** indicates significant p-values at $p < 0.001$. Black asterisks indicate significant change in all participants.

## 2.2 Cerebellar degeneration impairs connectivity with cerebellar regions

To understand the effects of cerebellar degeneration on the cortico-cerebellar motor network, we first examined functional connectivity at baseline. We quantified connectivity in a region-of-interest (ROI) approach as the Pearson's correlation between the resting-state time courses of neocortical regions involved in motor control (primary motor cortex, M1; dorsal premotor cortex, PMd; posterior parietal cortex, PPC) and the contralateral cerebellar motor region (hand region M3) for both left and right (see 4.4.2). We tested for significant effects of group (patient, control), regions (cortico-cortico, cortico-cerebellar, and cerebello-cerebello) and a group x region interaction using a linear mixed effects model (see 4.5). Patients showed significantly reduced connectivity at baseline (main effect of group: $F_{1,79} = 4.73, p = 0.03$; Fig. 3A) and this reduction depended on the region (group x region interaction: $F_{2,158} = 162.55, p = 4.52 \times 10^{-39}$). Specifically, connectivity with cerebellar motor regions was lower in patients, while cortico-cortico connectivity remained intact (corrected two-sample t-test patients-control difference; cortico-cerebellar: $t_{77} = -3.07, p = 0.02$; cerebellar-cerebellar connectivity: $t_{77} = -2.73, p = 0.02$; cortico-cortico: $t_{77} = 0.51, p = 1.00$; Fig. 3B). Connectivity across all participants differed between regions (main effect of regions: $F_{2,158} = 7.46, p = 8.02 \times 10^{-4}$), with strongest connectivity between the neocortical hemispheres, followed by cerebello-cerebello connectivity and, finally, weakest connectivity between neocortex and cerebellum (all pairwise comparisons significant at $t_{156} > 3.03, p < 5.12 \times 10^{-3}$).

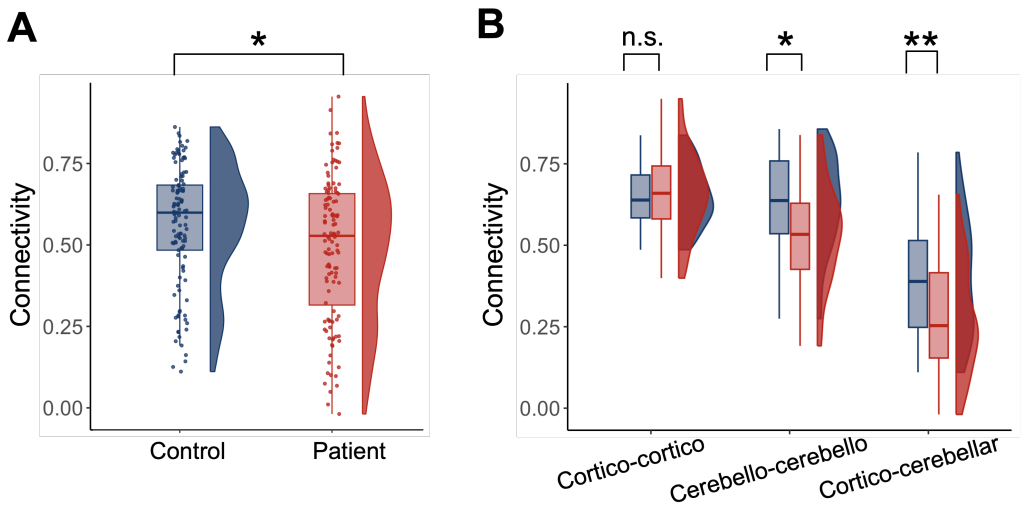


**Figure 3.** Impaired connectivity in the visuomotor network of patients. **A.** Connectivity of the visuomotor network differs at baseline between patients (red) and patients (blue). **B.** Connectivity shown separately for cortico-cortico, cerebello-cerebello and cortico-cerebellar connectivity shows that connectivity reduction in patients is specific to connectivity with cerebellar regions. * indicates significant p-values at $p < 0.05$. ** indicates significant p-values at $p < 0.01$. Black asterisks indicate significant change in all participants.

### 2.3 Training with visual feedback strengthens connectivity with bilateral premotor cortex in patients

Having established that cerebellar degeneration reduces connectivity in the cortico-cerebellar motor network, we then examined if prolonged training could reverse these impairments. We first examined training effects on connectivity with the dorsal premotor cortex (PMd), an area which has been shown to increase in grey matter through training in patients with cerebellar degeneration [6, 22]. We modelled connectivity of PMd contralateral to the training hand with a cerebellar motor region ipsilateral to the training hand in a linear mixed effects model with fixed effects of group, session, vision (vision / no vision) and feedback (explicit feedback / no explicit feedback), and included all higher-order interaction terms, along with a random effect of subject. We observed a significant patient-control difference in connectivity (main effect group: $F_{1,78.76} = 5.03, p = 0.03$; Fig. 4A). We also found a significant change in PMd-cerebellar connectivity (main effect session: $F_{1,78.15} = 8.33, p = 5.04 \times 10^{-3}$), with higher connectivity after training in all participants (pre: 0.32 ± 0.21, post: 0.38 ± 0.23). We found that PMd-cerebellar connectivity changed depended on vision (session x vision interaction: $F_{1,78.15} = 8.11, p = 5.63 \times 10^{-3}$), where participants who received visual feedback during training showed a significant increase in connectivity (vision: $t_{38} = -3.86, p = 8.50 \times 10^{-4}$), whereas participants without visual feedback showed no significant change (no vision: $t_{38} = -0.06, p = 0.94$). We observed no other significant main effects or higher-order interactions (all $F < 2.79, p > 0.1$).

Previous investigations of training-related changes in PMd have reported grey matter increases ipsilateral to the training hand that were greater in patients than in controls [22]. We therefore assessed connectivity changes between right PMd and a left cerebellar motor region. We found that connectivity between right PMd and a left cerebellar motor region differed between groups ($F_{1,78.82} = 7.47, p = 7.75 \times 10^{-3}$, patients: 0.30 ± 0.23, controls: 0.40 ± 0.20, Fig. 4B), but there was no overall connectivity change ($F_{1,78.20} = 0.99, p = 0.32$). However, a significant interaction between group, session and vision indicated that connectivity change depended on group and visual feedback (group x session x vision interaction: $F_{1,78.20} = 5.746, p = 0.01$). Specifically, patients showed increases in connectivity when training with vision ($t_{19} = -3.18, p = 0.02$), but connectivity did not change in healthy controls training with vision ($t_{18} = -0.53, p = 0.72$), or in patients training without vision ($t_{19} = -0.37, p = 0.72$).

To test the specificity of our findings to cortico-cerebellar connectivity, we performed a control analysis on inter-hemispheric connectivity calculated between left PMd and right PMd. As expected,

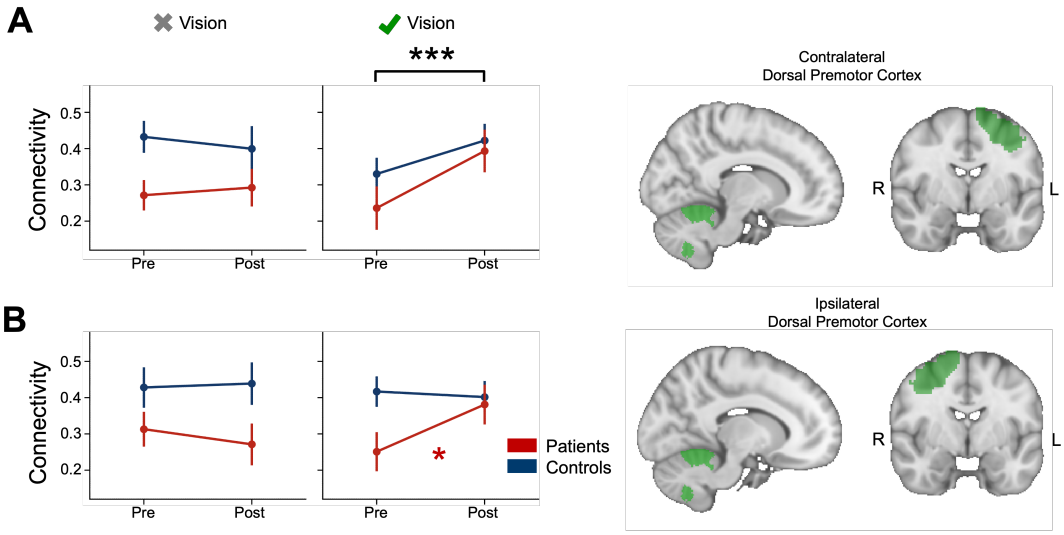


**Figure 4.** Connectivity change between dorsal premotor cortex (PMd) and cerebellar motor regions for training with and without vision. **A.** Left PMd connectivity with right cerebellar motor region. **B.** Right PMd connectivity with left cerebellar motor region. * indicates significant p-values at $p < 0.05$. *** indicates significant p-values at $p < 0.001$. Black asterisks indicate significant change in all participants, red asterisks indicate significant change for cerebellar patient group only.

we found no patient-control difference ($F_{1,78.97} = 1.99, p = 0.16$), no significant change in connectivity ($F_{1,78.67} = 2.85, p = 0.1$) and no effect of vision on connectivity change ($F_{1,78.97} = 0.12, p = 0.73$). These control analyses confirmed that vision-dependent changes in PMd connectivity were specific to connectivity with cerebellar motor regions.

### 2.4 Training with visual feedback increases cerebellar connectivity with contralateral posterior parietal cortex

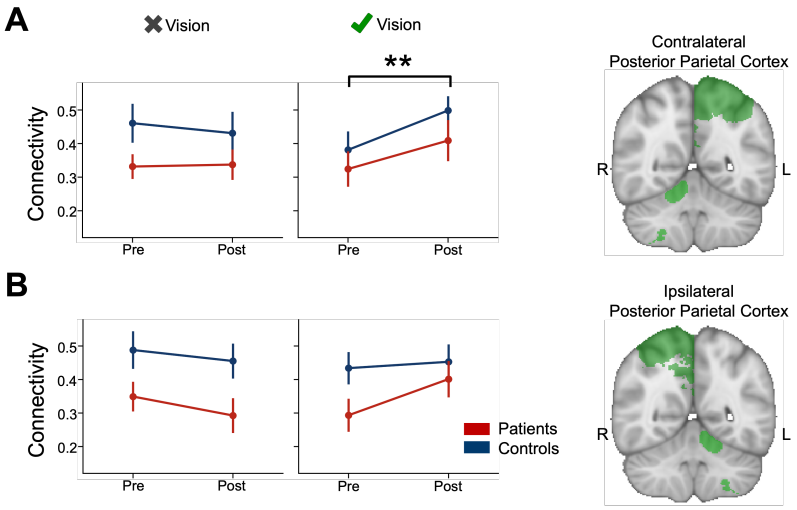


**Figure 5.** Connectivity change between posterior parietal cortex (PPC) and cerebellar motor regions when training with and without vision. **A.** Left PPC connectivity with cerebellar motor regions in the right hemisphere. **B.** Right PPC connectivity with cerebellar motor regions in the left hemisphere. * indicates significant p-values at $p < 0.05$. ** indicates significant p-values at $p < 0.01$. Black asterisks indicate significant change in all participants.

In light of the key role the posterior parietal cortex plays in re-calibrating visually guided reaching movements [48], we set out to test whether cerebellar connectivity with the posterior parietal cortex (PPC) increased when visual feedback was provided during training. We observed a significant difference in connectivity between patients and healthy control participants, with reduced connectivity in patients compared to controls ($F_{1,78.96} = 4.85, p = 0.03$; patients: 0.35 ± 0.21, controls: 0.44 ± 0.23; Fig. 5A). Connectivity between left PPC and right cerebellar motor region changed through training overall, with higher connectivity after training ($F_{1,78.30} = 4.95, p = 0.03$; pre: 0.37 ± 0.22, post: 0.42 ± 0.23). Connectivity also changed as a function of visual feedback ($F_{1,78.30} = 7.21, p = 0.01$). All participants who received visual feedback showed increased left PPC - right cerebellar connectivity after training (vision: $t_{38} = -3.27, p = 4.52 \times 10^{-3}$; no vision: $t_{38} = -0.31, p = 0.76$).

Ipsilateral to the training hand, PPC connectivity with contralateral cerebellum showed a significant patient-control difference at baseline ($F_{1,79.23} = 9.11, p = 3.42 \times 10^{-3}$; Fig. 5B), but no connectivity change from baseline ($F_{1,78.70} = 0.26, p = 0.61$). Although a significant vision x session interaction indicated that vision affected connectivity change between these regions ($F_{1,78.70} = 5.94, p = 0.02$), post hoc comparisons could not determine which condition drove this change (vision: $t_{38} = 1.51, p = 0.13$, no vision: $t_{38} = -1.82, p = 0.13$). A control analysis of left and right PPC connectivity found no patient-control differences ($F_{1,79.34} = 0.58, p = 0.45$), and no change in connectivity overall or as a function of visual feedback ($F_{1,79.34} = 1.28, p = 0.26$). Taken together, these results confirm the specificity of our findings to PPC-cerebellar connectivity.

### 2.5 Motor training increases connectivity with contralateral primary motor cortex

Motor training has been shown to change connectivity between left M1 and right cerebellar cortex [49, 50]. We tested whether practicing reaching movements, irrespective of training condition, changes functional connectivity between the right cerebellar and left M1 hand region. Indeed, we found that contralateral to the right hand, M1-cerebellar connectivity increased through training ($F_{1,77.86} = 4.64, p = 0.03$; Fig. 6A), such that connectivity was higher after training (pre: 0.22 ± 0.19; post: 0.27 ± 0.19). There was a significant patient-control difference in connectivity ($F_{1,78.29} = 8.69, p = 4.21 \times 10^{-3}$), but no difference in connectivity change between patients and controls (group x session interaction: $F_{1,77.86} = 0.03, p = 0.86$). Previous studies indicated that M1-cerebellar connectivity change depended on learning [50] but we did not find any studies that tested the influence of visual or explicit feedback. We found no effect of vision or explicit feedback on connectivity change (vision x session: $F_{1,77.86} = 3.34, p = 0.07$, explicit feedback x session: $F_{1,77.86} = 0.41, p = 0.52$).

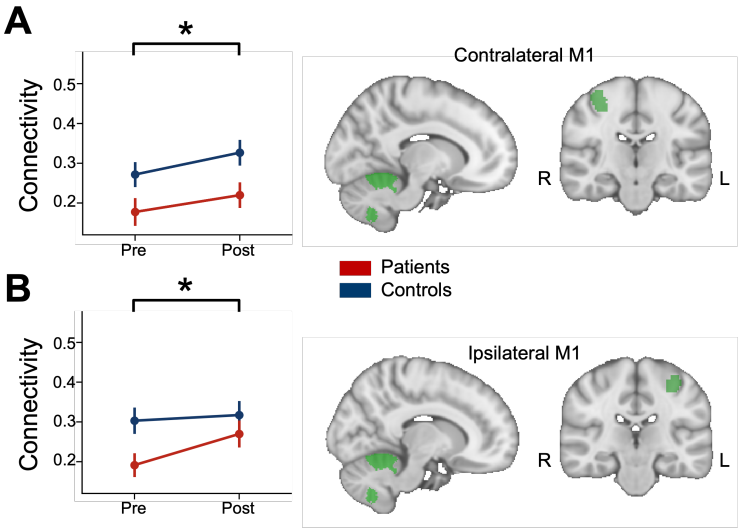


**Figure 6.** Connectivity change between M1 and cerebellar motor regions. **A.** Left M1 connectivity with right cerebellar motor region. **B.** Right M1 connectivity with left cerebellar motor region. * indicates significant p-values at $p < 0.05$. Black asterisks indicate significant change in all participants.

To test for the specificity of our findings to M1 contralateral to the training hand, we tested for

connectivity changes from baseline of right M1 - left cerebellar connectivity. We found no significant connectivity change from baseline overall, suggesting that the training-related increase was specific to connectivity between left M1 and right cerebellar hand region ($F_{1,78.46} = 3.78, p = 0.06$; Fig. 6B). We also examined connectivity between the neocortical hemispheres for the M1 hand regions. Here, we observed no connectivity difference overall ($F_{1,78.92} = 2.91, p = 0.09$), but a significant increase in connectivity between left and right M1 ($F_{1,78.63} = 5.05, p = 0.03$).

Finally, we tested for a change in connectivity between left and a right cerebellar motor region through training or as a function of feedback. Our analysis showed a difference in connectivity between patients and controls at baseline ($F_{1,78.97} = 5.77, p = 0.02$). We also found a significant change in connectivity from baseline to post-training for all participants ($F_{1,78.47} = 8.13, p = 5.571 \times 10^{-3}$). This change depended on explicit feedback ($F_{1,78.63} = 5.40, p = 0.02$), but not on vision, group, or an interaction between these factors (all $F < 1.60, p > 0.20$). Thus, we cannot conclude that the overall change in M1-cerebellar connectivity was specifically driven by strengthening of cortico-cerebellar connectivity. However, the lack of significant higher-order interactions with vision suggest that our findings of PMd-cerebellar connectivity and PPC-cerebellar connectivity increases through training with vision are not driven by an increase in connectivity between cerebellar motor regions.

### 2.6 Explicit feedback affects connectivity in cognitive cortico-cerebellar network

Cognitive regions of the neocortex have been implicated in strategy forming and explicit learning during visuomotor reaching tasks [51, 52, 53]. We therefore explored how explicit verbal feedback during training would affect connectivity between cognitive regions of the neocortex and the cerebellum. For this, we chose a region of interest from a novel functional atlas of the cerebellum, which was based on an aggregate of 7 extensive functional datasets [54]. We chose region D2 from the cerebellar atlas, which is a core multiple demand region that activates during the rapid processing of instructive signals in motor tasks [54] and is located in lobules VI and VII along the superior posterior and the ansoparamedian fissures. We examined connectivity of D2 with the right dorsolateral prefrontal cortex (dlPFC), known to engage during strategy-based learning in adaptive reaching

We observed a significant interaction between group, session and feedback ($F_{1,78.83} = 5.09, p = 0.03$; Fig. 7). Although paired t-tests of connectivity before and after training showed a significant decrease in connectivity for patients when training with explicit feedback ($t_{19} = -2.14, p = 0.04$), but not without ($t_{19} = -1.05, p = 0.31$) these tests did not reach statistical significance when corrected for multiple comparisons (corrected p-values: $p = 0.18$ in feedback conditions, $p = 0.42$ in no feedback conditions). For connectivity between right dlPFC and left D2 or connectivity between left D2 and right D2, we found no significant interaction between group, session and feedback (right dlPFC - left cerebellar motor region: $F_{1,79.00} = 3.95, p = 0.05$; right D2 - left D2: $F_{1,78.70} = 0.08, p = 0.78$). Thus, any feedback-dependent effects on connectivity changes in patients and controls appear specific to right dlPFC connectivity with a right cerebellar cognitive region.

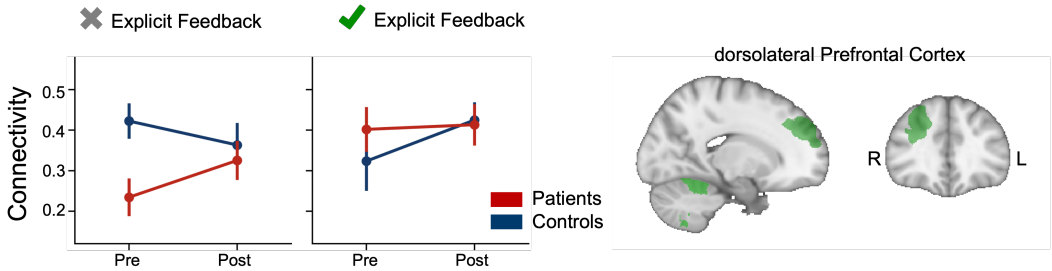


**Figure 7.** Connectivity change between right dorsolateral prefrontal cortex (dlPFC) and right cognitive cerebellar region (cerebellar atlas region D2 in Nettekoven et al., 2023 [54]) training where explicit verbal feedback was given or not.

## 3 DISCUSSION

How cerebellar degeneration affects cortico-cerebellar connectivity and how therapeutic interventions can counter these effects are key clinical and neuroscientific questions that have yet to be addressed. In

this study, we used a newly developed and carefully validated neuroimaging pipeline to demonstrate, for the first time, cortico-cerebellar connectivity alterations in cerebellar patients that ameliorate with training in a feedback-dependent manner. The main findings of the study are: First, at baseline, patients showed reduced connectivity of cerebellar motor regions with contralateral neocortical and cerebellar regions, while cortico-cortico connectivity was unimpaired. Second, visuomotor training led to increased connectivity between cerebellar motor and PMd contralaterally to the trained arm for all participants and ipsilaterally to the training arm for patients. Third, training with visual feedback increased connectivity with the PPC in all participants. These findings were highly specific to cortico-cerebellar connectivity. They were not driven by changes in neocortical connectivity, as left-right PMd connectivity and left-right PPC connectivity did not change overall.

To date, plastic changes after training interventions in cerebellar patients have only been demonstrated in regions not directly affected by degeneration [6], including in a previous report of structural changes in this cohort [22]. These previous studies found grey matter increases in PMd, but were unable to demonstrate changes in cerebellar grey matter.

Increased temporal synchrony of resting-state fluctuations in distant brain regions are thought to reflect increased communication of these regions [55, 56]. This connectivity increase could be driven by strengthening of connections between brain regions involved in training, which remain detectable at rest post-training. In line with this, connectivity increases between task-relevant regions have been demonstrated in the visual cortex [57], motor cortex [58] and cerebellar cortex [59, 60]. Given that the cerebellum projects to PMd [61], our findings indicate that visuomotor training can take advantage of residual connections in the cortico-cerebellar network and induce lasting changes in the communication between the training-relevant regions.

The execution of visually guided movements involves the PPC [62]. In line with this, we find that during visuomotor training, functional connectivity between a cerebellar motor region and PPC increases contralateral to the training hand. Strengthening of a network involving cerebellar regions and contralateral PPC has previously been reported in response to motor adaptation in healthy participants [63]. To our knowledge, our study is the first to demonstrate connectivity changes involving the PPC in cerebellar patients as well as healthy controls.

Previous research has found strengthening of connectivity between cerebellum and M1 contralateral to the training hand, when adaptive learning takes place, but not when no learning was induced [50]. This M1-cerebellar connectivity change, assessed through paired-pulse transcranial magnetic stimulation measures of cerebellar-brain inhibition, appears to rely on the presence of larger movement errors and does not manifest when introducing systematic errors gradually or randomly [49]. Here, we found M1-cerebellar resting-state connectivity increased regardless of task condition. These findings are in line with prior work, since all task conditions in this study tended to induce similar rates of learning, with differences between conditions appearing only in some target directions [22]. Moreover, the training conditions in this study were matched in all aspects of training protocol apart from visual and explicit verbal feedback, which have so far not been reported to induce differential changes in M1-cerebellar connectivity.

When exploring changes in a cortico-cerebellar network involved in higher-order cognitive aspects of motor training, we observed changes that differed between patients and controls and depended on the presence of explicit feedback. While these differences appear to be driven by a connectivity increase in the patient group when training without explicit feedback, post hoc tests did not survive multiple comparisons. Although these findings might point to a potential malleability of cognitive cortico-cerebellar connectivity through targeted interventions, they will need to be replicated in an independent sample.

We were able to reveal highly specific connectivity changes by optimizing our analysis pipeline for maximising overlap of cerebellar structures and thereby preserving cerebellar signal. By creating a novel template for the analysis of cerebellar patient data, the *DeCon* template, we reduced spatial spread of anatomical landmarks in the cerebellum by 30-70% from existing templates, including the MNI template and the SUIT template, which had so far been the gold standard in cerebellar neuroimaging analysis [64]. When training a noise classifier on cerebellar resting-state fMRI data, mapping to MNI standard space via the DeCon template in a multi-stage deformation tripled classification accuracy. To enable other researchers to take advantage of this methodological advancement, we are making the template freely available under `https://github.com/carobellum/DegenerationControlTemplate`. We believe that it will improve anatomical and functional analysis of patient data and prove useful to

the research and clinical community.

### 3.1 Conclusions

Our results demonstrate, for the first time, that cortico-cerebellar connectivity can be ameliorated in cerebellar patients with training in a feedback-dependent manner. We used a newly developed and carefully validated brain template to reveal these subtle, but robust connectivity changes. These results demonstrate a fundamental step forward in understanding residual function in cerebellar degeneration patients and developing training protocols that take this knowledge into account. Further, the methodological advances presented here constitute a valuable addition to the tools available for cerebellar patient studies.

## 4 METHODS

### 4.1 Participants

41 patients with cerebellar degeneration and 44 neurologically healthy individuals participated in this study. One patient and two controls dropped out before study completion due to acute illness unrelated to the study, and two control participants were removed from analysis due to incidental findings, resulting in a final sample of 40 patients (age 55 ± 11.29 years, 21 females) and 40 age and sex-matched controls (age 55 ± 10.83 years, 20 females). For detailed study demographics, see Draganova et al., 2022 [22]. Patients were diagnosed with a pure form of cerebellar cortical degeneration. Predominant diagnosis were spinocerebellar ataxia type 6, autosomal dominant cerebellar ataxia type 3, and sporadic adult-onset ataxia of unknown etiology. Ataxia severity was assessed using the clinical Scale for the Assessment and Rating of Ataxia [65] (SARA). Participants were pseudo randomly assigned to one of four motor training conditions. Training groups were matched for sex, age and ataxia severity (SARA scores) and all participants were right-handed as assessed by the Edinburgh handedness scale [37]. The study was approved by the Ethics Committee of the Essen University Medical Center and all participants gave verbal and written informed consent prior to testing.

### 4.2 Motor training

-day motor training, participants performed elbow flexion movements in the horizontal plane using a single-joint manipulandum to targets arranged on a semicircular metal frame at 95 cm distance (Fig. 1A; manipulandum and task details can be found in [36, 22]). Participants began each trial in a start position of 90°elbow flexion. After the experimenter gave a start command, participants performed a single, ramp-like movement without online correction to the target. Participants held their arm in the end position for 4s before moving it back to the start position. Participants were instructed to perform swift and accurate movements. If movements were too slow or too fast according to previously calculated limits, the experimenter provided correctional feedback to reduce or increase movement speed.

On each training day, participants performed 100 trials to targets located counterclockwise at 10°and 50°, in blocks of 25 trials that alternated between the two targets. The target of the first block was balanced across participants of each training group and alternated each day. Participants began each training day by performing three familiarization trials to the first target of that day. After each block, participants rested for 3 minutes and after completing two blocks, participants relaxed their arm outside of the manipulandum.

To continuously drive performance, the width of the targets was reduced according to the movement accuracy achieved by the participant. Participants began at the lowest performance level with a target width of 4.5 cm, corresponding to 2.7°on the frame. After performing five consecutive movements where the beam of the laser pointer was on target, the target width was reduced to the next smaller width (4.5 cm/2.7°, 3.5 cm/2.11°, 2.5 cm/1.5°, 1.5 cm/0.9°, 0.5 cm/0.3°). Participants were instructed about the five levels prior to the experiment and notified by the experimenter as they advanced to the next level. Behavioural results have been reported previously [36, 22].

#### *4.2.1 Conditions*

Participants were pseudo-randomly assigned to one of four motor training conditions, varying online visual feedback (Vision/No Vision) and post-movement verbal feedback (Expl. Feedback / No Expl. Feedback). 10 patients and 10 controls performed each condition (Vision — No Vision — Vision + Expl. Feedback — No Vision + Expl. Feedback). In conditions without vision, participants wore a mask that fully occluded vision. Here, the experimenter guided the arm of the participant from the start position

to the target before each trial to enable the participant to memorize the target position. After moving back to the start position, participants performed the movement to the target. The experimenter informed participants verbally about the movement outcome, indicating whether the movement was "on target" or "target has not been reached". In conditions with explicit feedback, participants received verbal feedback after each movement about the final joint position relative to the target, and strategies to minimize future movement errors (i.e., "Target was undershoot by 5°. Increase movement by °degrees").

Each trial lasted 10s in the vision only condition and 15-20s when verbal feedback was given in addition to vision. In the conditions without vision, trials lasted 50-60s. Therefore, each training session with vision lasted 45-60 minutes, and 90-100 minutes without vision.

## 4.3 MRI acquisition

Magnetic resonance imaging data was collected on the days before and after training (Fig. 1B) on a 3T combined MRI-PET scanner (Siemens Healthcare, Erlangen, Germany) with a 16-channel head coil with the same scanning protocol. Structural MRI data was acquired using a magnetization-prepared rapid acquisition gradient echo (MPRAGE) sequence with the following parameters: TR = 2530 ms, TE = 3.26 ms, inversion time = 1100 ms, flip angle = 7; FOV = 256 x 256 x 176mm$^3$; bandwidth = 200 Hz/pixel; GRAPPA acceleration factor 2 and 48 reference lines; whole brain, acquisition time = 6:24 min. Resting-state fMRI data was acquired with the following parameters: TR/TE = 3000/35 ms, FOV = 282 x 282 x 134 mm$^3$, bandwidth = 2312 Hz/pixel, voxel dimension = 3x3x2.7 mm$^3$, GRAPPA acceleration factor 3 and 90 reference lines, whole brain, acquisition time = 5:17 min for a total of 100 volumes. During resting-state fMRI acquisition, participants fixated on a cross-hair image presented centrally on the screen. No functional data was acquired for one healthy control participant at both timepoints and for another healthy control participant at timepoint post due to scanner failure. The first subject was therefore excluded from functional analysis, while the second one was included for baseline connectivity but excluded for connectivity change analysis.

## 4.4 MRI Analysis

All MRI data was processed using the Functional MRI of the Brain Software Library, (FSL; version 6.0.4; [66]). Structural images were additionally processed using advanced normalization tools (ANTs)[67] and ITK-SNAP[68].

### *4.4.1 Structural MRI analysis*

Structural images were reoriented to standard MNI orientation, cropped to remove superfluous neck tissue and corrected for RF/B1 field inhomogeneities using FSL's fsl_anat [66]. Brain masks were generated using the Optimized Brain Extraction for Pathological Brains (optiBET [69]). To ensure precise tracing of the border between brain and non-brain tissue, in particular for degenerated brains, brain masks were corrected by hand by an experienced technician otherwise blinded to the study. Using the hand-corrected masks, the structural images were skull-stripped.

**Template Generation** Given the anatomical abnormalities present in brains with cerebellar degeneration and in scans of older adults [38, 39, 30, 40, 41, 42, 43, 44], it was important to use a registration template that is appropriate for patient brains and older adults. We therefore constructed a study-specific template from the scans of 40 participants. The other half of the sample was held out for validation purposes (see 4.4.1). Scans that showed highly abnormal anatomy or particularly severe pathology, such as enlarged ventricles or strongly degenerated cerebellum, were not used for template generation, but included in the validation sample. To avoid biasing the template to a specific group or training condition, the template was constructed from twenty patient and twenty healthy control brains balanced across conditions (see Supplementary Table 1). Additionally, the scans were chosen to be representative of the mean sample age and sex distribution and balanced across scan time points.

The study-specific template was generated from the brain-extracted structural images using the iterative process implemented by the advanced normalization tools (ANTs, antsMultivariateTemplateConstruction2, [67]). As a starting point for the template construction, an existing group template derived from brains aged 55-59 was selected, which presented the closest match to the mean age of our sample (obtained from Neurodevelopmental MRI Database [70]). In brief, the structural images were rigidly, then linearly and finally nonlinearly registered to the starting template. The resampled images were averaged and deformed using the inverse average deformation to obtain a true mean shape image. This image served as the new

starting template for the next iteration. To optimize convergence, ANTs downsamples and smoothes the images before registration and repeats the iterative process at progressively finer resolution and smoothing kernels. Our template underwent five refinement stages at 8x6x4x2x1 mm image resolution, 6x4x2x1x0 voxel smoothing kernels, and 500x200x100x70x20 maximum iterations. We hereby created a new template for comparing degenerated brains with control brains (DegenerationControl template, DeCon). To obtain a mapping between the DeCon template and MNI template, the DeCon template was nonlinearly registered to the MNI template using antsRegistrationSyn. The resulting nonlinear warp field was converted to an fsl-compatible format using the c3d_affine_tool from ITK-SNAP[68] and FSL's fslulils [66].

All structural images were nonlinearly registered to the template using antsRegistrationSyn [67]. To enable comparisons between the DeCon template and existing templates, we additionally nonlinearly registered the structural images to the MNI template[45] (nonlinear 6th generation MNI152 template or MNI152NLin6Asym available at `https://www.templateflow.org/`, hereafter referred to as 'MNI template') and the SUIT template [33] using antsRegistrationSyn [67], all at 1mm resolution ( with precision type set to float and histogram matching turned on and all other parameters set to default values). Registration to the SUIT template was performed after isolating the cerebellum from the surrounding tissue in the structural scan using the SUIT isolate function [33].

**Template Validation** We evaluated the degree of anatomical correspondence between cerebella in group space by calculating the spatial spread of anatomical landmarks of the cerebellum, using a procedure established by Diedrichsen, 2006[33]. As landmarks, we chose two major fissures, the primary fissure separating lobules V and VI and the intrabiventer fissure VIIIa and VIIIb. Fissures were drawn as surfaces on the structural scans in native space of each participant by an experienced technician otherwise blinded to the study. The fissures were then resampled to DeCon space, SUIT space and MNI space. Spatial overlap was calculated as the average distance between corresponding fissures of each possible pair of participants. Specifically, we computed the smallest distance of each point of fissure A to a point on the fissure B and averaged these first across all points of the fissure A, and then across all participants. Fissure alignment was calculated both for the entire cerebellum, using a cerebellar mask in group space, and restricted to the vermal section, using a mask obtained from the SUIT atlas [71].

As a second evaluation criterion, we compared the ability of the automated noise classifier FIX [47] to identify noise components of functional data using structural-to-MNI registrations estimated either directly to MNI space or with the DeCon template as an intermediate step. Since noise driven by vein fluctuations is dissociable from neural signal only by voxel location in major draining veins, FIX uses MNI-space masks of the major veins resampled to native functional space to identify vein noise [47]. Thus, FIX's ability to detect noise relies in part on an accurate mapping between MNI space and native functional space. We therefore compared FIX's classification accuracy using functional-to-MNI registrations estimated directly or via the DeCon template (see 4.4.2).

#### *4.4.2 Functional MRI analysis*

The resting-state functional MRI data acquired before and after the training days was preprocessed using steps largely matched to the UK Biobank processing pipeline [72]. The data was motion corrected using MCFLIRT [66], slice-timing corrected using Fourier-space time series phase-shifting, stripped of non-brain voxels using BET (Brain Extraction Tool; [73]) and high-pass temporally filtered with a cut off frequency of 100s. No spatial smoothing was applied. Functional data were registered to the MNI space via the DeCon template and the structural scan of each subject and session. To this end, functional data were first linearly registered to the subject's structural image acquired in the same session using boundary-based registration (implemented in FLIRT, [74, 75, 76]). The linear transformation was concatenated with the structural-to-DeCon nonlinear warp field and the DeCon-to-MNI nonlinear warp field into a functional-to-MNI space warp field.

**FIX Training** Structured noise was removed from functional data using a single-subject independent component analysis (ICA), implemented in MELODIC (Multivariate Exploratory Linear Optimized Decomposition into Independent Components) and the automated classifier FIX [47]. Because existing labelled training datasets differ substantially in their study population and acquisition parameters from our data, we created our own training set by manually classifying a subset of the scans [77, 47]. We selected 41 of the 157 scans in the dataset (26%), balanced across groups, conditions and timepoints for hand classification. To avoid optimizing our analysis pipeline to any particular set of scans, we minimized

overlap between scanning sessions selected for template generation and for hand classification, with scans from eight subjects and timepoints included in both.

**FIX Evaluation** Classification accuracy was evaluated using leave-one-subject-out cross-validation where ICA components from a single hand-labelled subject are left out of the training process and the classification accuracy is then tested on the left-out subject [47]. Classification accuracy was summarized in terms of true positive rate ("TPR"), i.e. the percentage of correctly detected signal components, and true negative rate ("TNR"), i.e. the percentage of correctly detected noise components. A commonly used overall performance measure was calculated as the weighted average of TPR and TNR: $(3*TPR+TNR)/4$ [47, 78, 79]. Since FIX provides probabilistic signal and noise assignments and applies a threshold to obtain a binary assignment, classification accuracy was evaluated over a range of thresholds (threshold of 1, 2, 5, 10, 20, 30, 40 and 50). Since leave-one-out testing showed highest overall performance at threshold 30 (91.2 % accuracy), noise components identified at threshold 30 were removed from the functional data using FIX unique variance cleanup.

**Functional connectivity** We quantified functional connectivity between neocortex and cerebellum using a region of interest (ROI)-based approach for motor regions and regions involved in cognitive aspects of motor planning. For the neocortex, we derived an ROI of the left and right primary motor cortex (M1) hand area based on previous functional MRI data of hand movements [80]. A dorsal premotor cortex ROI (PMd) was defined for the left and right hemisphere from a tractography-based atlas [81]. A posterior parietal cortex (PPC) ROI was defined as left and right area 7 of the Juelich histological atlas [82] thresholded at 15. Finally we defined an ROI for the right dorsolateral prefrontal cortex (dlPFC) as area 46d of the Sallet atlas [83] thresholded at 25.

To define cerebellar ROIs, we used a novel functional atlas of the cerebellum based on multiple fMRI datasets that parcellates the cerebellum into 32 symmetrical functional regions [54]. We defined cerebellar motor ROIs as the left and right hand motor regions M3L and M3R, which activate strongly in response to movements of the ipsilateral hand. To explore connectivity changes in cerebellar cognitive regions in response to explicit verbal feedback, we used regions D2L and D2R. D2 was chosen because it shows highest activity during rapid processing of instructive signals in a motor task (see Supplementary Figure S2 in Nettekoven et al., 2023) and its specific involvement in working memory recall [84], a cognitive function that deteriorates in cerebellar degeneration [85]. D2 also functionally connects to prefrontal regions of the neocortex [54].

We quantified functional connectivity as the Pearson's correlation coefficient between the resting-state time courses of two ROIs. To ensure normality, we used Fisher's r-to-z-transformation on the connectivity values. For visualization purposes, we used non-normalized connectivity values.

## 4.5 Statistical analysis

Mean ± SD is presented throughout. Statistical analyses were conducted using R (version 4.3.1 [86]) and Python (version 3.9.10). We used paired t-tests to test for differences in fissure alignment and noise identification (scipy version 1.12.0 [87]).

To test for connectivity differences at baseline, we constructed a linear mixed effects model of baseline connectivity values using the lme4 package (version 1.1-35.1). We averaged connectivity values within subject across regions, such that each subject had one cortico-cortico, one cortico-cerebello and one cerebello-cerebello connectivity value. We included fixed effects of group (patient, control), region (cortico-cortico, cortico-cerebello, cerebello-cerebello) and a group x region interaction term.

To investigate changes in functional connectivity and how these depend on group and training condition, we constructed separate linear mixed effects models for each pair of ROIs. We included timepoint, group, vision and feedback as fixed effects, along with their higher-order interaction terms. We allowed intercepts for different subjects to vary in the linear mixed effects models, to account for covarying residuals within subjects. Separate models of connectivity with M1, PMd, PPC and dlPFC were constructed, as the hypotheses regarding the specific fixed effects of interest were different for different regions. Residuals of all linear models were confirmed to be homoscedastic by visually inspecting the residuals plotted against the predicted values of each independent variable. Normality of fixed effects residuals and random effect residual was confirmed by visual inspection of the Q-Q plot using the ggpubr package (version 0.6.0). P-values were obtained with Type III tests calculated with Satterthwaite's method (alpha = 0.05) implemented in the lmerTest package (version 3.1.3) [88]. In models with significant

interactions, pairwise differences were assessed at each level using independent t-tests for patient-control differences and paired t-tests for comparing connectivity before and after training. P-values for post hoc tests were corrected for multiple comparisons using the Benjamini–Hochberg method [89], where all patient-control comparisons or all pre-post comparisons formed one family of tests. For testing connectivity differences at baseline, region combinations formed a family of tests. Since tests between regions are not independent, we corrected for multiple comparisons using the Benjamini-Yekutieli method [90], as this method does not assume independence of tests.

## REFERENCES


[1] Jürgen Konczak, Daniela Pierscianek, Sarah Hirsiger, Uta Bultmann, Beate Schoch, Elke R. Gizewski, Dagmar Timmann, Matthias Maschke, and Markus Frings. Recovery of upper limb function after cerebellar stroke: Lesion symptom mapping and arm kinematics. *Stroke*, 2010.

[2] Mario Manto and Daniele Marmolino. Cerebellar ataxias. *Current Opinion in Neurology*, 2009.

[3] D. Marmolino and M. Manto. Past, Present and Future Therapeutics for Cerebellar Ataxias. *Current Neuropharmacology*, 8(1):41–61, 2010.

[4] W. Ilg, A. J. Bastian, S. Boesch, R. G. Burciu, P. Celnik, J. Claaßen, K. Feil, R. Kalla, I. Miyai, W. Nachbauer, L. Schöls, M. Strupp, M. Synofzik, J. Teufel, and D. Timmann. Consensus paper: Management of degenerative cerebellar disorders, 2014.

[5] Winfried Ilg and Dagmar Timmann. General Management of Cerebellar Disorders: An Overview. In *Handbook of the Cerebellum and Cerebellar Disorders: Second Edition: Volume 3*. 2021.

[6] Roxana Gabriela Burciu, Nicole Fritsche, Oliver Granert, Lutz Schmitz, Nina Spönemann, Jürgen Konczak, Nina Theysohn, Marcus Gerwig, Thilo van Eimeren, and Dagmar Timmann. Brain changes associated with postural training in patients with cerebellar degeneration: A voxel-based morphometry study. *Journal of Neuroscience*, 33(10):4594–4604, 2013.

[7] W. Ilg, M. Synofzik, D. Brötz, S. Burkard, M. A. Giese, and L. Schöls. Intensive coordinative training improves motor performance in degenerative cerebellar disease. *Neurology*, 2009.

[8] Winfried Ilg, Cornelia Schatton, Julia Schicks, Martin A. Giese, Ludger Schöls, and Matthis Synofzik. Video game-based coordinative training improves ataxia in children with degenerative ataxia. *Neurology*, 2012.

[9] Jennifer L. Keller and Amy J. Bastian. A home balance exercise program improves walking in people with cerebellar ataxia. *Neurorehabilitation and Neural Repair*, 2014.

[10] Ichiro Miyai, Mizuki Ito, Noriaki Hattori, Masahito Mihara, Megumi Hatakenaka, Hajime Yagura, Gen Sobue, and Masatoyo Nishizawa. Cerebellar ataxia rehabilitation trial in degenerative cerebellar diseases. *Neurorehabilitation and Neural Repair*, 2012.

[11] Amy J. Bastian. Learning to predict the future: the cerebellum adapts feedforward movement control, 2006.

[12] Nicola Saywell and Denise Taylor. The role of the cerebellum in procedural learning - Are there implications for physiotherapists' clinical practice?, 2008.

[13] W. Thomas Thach and Amy J. Bastian. Role of the cerebellum in the control and adaptation of gait in health and disease. *Progress in Brain Research*, 2004.

[14] Matthias Maschke, Christopher M. Gomez, Timothy J. Ebner, and Jürgen Konczak. Hereditary Cerebellar Ataxia Progressively Impairs Force Adaptation during Goal-Directed Arm Movements. *Journal of Neurophysiology*, 2004.

[15] James R. Bloedel. Cerebellar afferent systems: A review. *Progress in Neurobiology*, 1973.

[16] Nasir H. Bhanpuri, Allison M. Okamura, and Amy J. Bastian. Active force perception depends on cerebellar function. *Journal of Neurophysiology*, 2012.

[17] Publisher Taylor. Ac ce pt. (October):37–41, 2014.

[18] Jordan A. Taylor, John W. Krakauer, and Richard B. Ivry. Explicit and implicit contributions to learning in a sensorimotor adaptation task. *Journal of Neuroscience*, 34(8):3023–3032, 2014.

[19] Jordan A. Taylor, Nola M. Klemfuss, and Richard B. Ivry. An explicit strategy prevails when the cerebellum fails to compute movement errors. *Cerebellum*, 9(4):580–586, 2010.

[20] John D. Fryer, Peng Yu, Hyojin Kang, Caleigh Mandel-Brehm, Angela N. Carter, Juan Crespo-Barreto, Yan Gao, Adriano Flora, Chad Shaw, Harry T. Orr, and Huda Y. Zoghbi. Exercise and genetic rescue of SCA1 via the transcriptional repressor Capicua. *Science*, 2011.

[21] Adeel Safdar, Jacqueline M. Bourgeois, Daniel I. Ogborn, Jonathan P. Little, Bart P. Hettinga, Mahmood Akhtar, James E. Thompson, Simon Melov, Nicholas J. Mocellin, Gregory C. Kujoth, Tomas A. Prolla, and Mark A. Tarnopolsky. Endurance exercise rescues progeroid aging and induces systemic mitochondrial rejuvenation in mtDNA mutator mice. *Proceedings of the National Academy of Sciences of the United States of America*, 2011.

[22] Rossitza Draganova, Frank Konietschke, Katharina M. Steiner, Naveen Elangovan, Meltem Gümüs, Sophia M. Göricke, Thomas M. Ernst, Andreas Deistung, Thilo van Eimeren, Jürgen Konczak, and Dagmar Timmann. Motor training-related brain reorganization in patients with cerebellar degeneration. *Human Brain Mapping*, 43(5):1611–1629, 2022.

[23] Carlos R. Hernandez-Castillo, Sarael Alcauter, Victor Galvez, Fernando A. Barrios, Petra Yescas, Adriana Ochoa, Lizbeth Garcia, Rosalinda Diaz, Wei Gao, and Juan Fernandez-Ruiz. Disruption of visual and motor connectivity in spinocerebellar ataxia type 7. *Movement Disorders*, 28(12):1708–1716, 2013.

[24] Elinor Tzvi, Christoph Zimmermann, Richard Bey, Thomas F. Münte, Matthias Nitschke, and Ulrike M. Krämer. Cerebellar degeneration affects cortico-cortical connectivity in motor learning networks. *NeuroImage: Clinical*, 16(July):66–78, 2017.

[25] Ian H. Harding, Louise A. Corben, Elsdon Storey, Gary F. Egan, Monique R. Stagnitti, Govinda R. Poudel, Martin B. Delatycki, and Nellie Georgiou-Karistianis. Fronto-cerebellar dysfunction and dysconnectivity underlying cognition in friedreich ataxia: The IMAGE-FRDA study. *Human Brain Mapping*, 2016.

[26] N. Georgiou-Karistianis, H. Akhlaghi, L. A. Corben, M. B. Delatycki, E. Storey, J. L. Bradshaw, and G. F. Egan. Decreased functional brain activation in Friedreich ataxia using the Simon effect task. *Brain and Cognition*, 79(3):200–208, 2012.

[27] Andrew Zalesky, Hamed Akhlaghi, Louise A. Corben, John L. Bradshaw, Martin B. Delatycki, Elsdon Storey, Nellie Georgiou-Karistianis, and Gary F. Egan. Cerebello-cerebral connectivity deficits in Friedreich ataxia. *Brain Structure and Function*, 219(3):969–981, 2014.

[28] Carlos R. Hernandez-Castillo, Víctor Galvez, Consuelo Morgado-Valle, and Juan Fernandez-Ruiz. Whole-brain connectivity analysis and classification of spinocerebellar ataxia type 7 by functional MRI. *Cerebellum and Ataxias*, 1(1):1–8, 2014.

[29] Alan C. Evans, Andrew L. Janke, D. Louis Collins, and Sylvain Baillet. Brain templates and atlases. *NeuroImage*, 62(2):911–922, 2012.

[30] Catriona D. Good, Ingrid S. Johnsrude, John Ashburner, Richard N.A. Henson, Karl J. Friston, and Richard S.J. Frackowiak. A voxel-based morphometric study of ageing in 465 normal adult human brains. *NeuroImage*, 2001.

[31] John Ashburner and Karl J. Friston. Voxel-based morphometry - The methods. *NeuroImage*, 2000.

[32] Paul M. Thompson, Michael S. Mega, Roger P. Woods, Chris I. Zoumalan, Chris J. Lindshield, Rebecca E. Blanton, Jacob Moussai, Colin J. Holmes, Jeffrey L. Cummings, and Arthur W. Toga. Cortical change in Alzheimer's disease detected with a disease-specific population-based brain atlas. *Cerebral Cortex*, 2001.

[33] Jörn Diedrichsen. A spatially unbiased atlas template of the human cerebellum. *NeuroImage*, 33(1):127–138, 2006.

[34] Benjamin B. Risk, Mary C. Kociuba, and Daniel B. Rowe. Impacts of simultaneous multislice acquisition on sensitivity and specificity in fMRI. *NeuroImage*, 172(February):538–553, 2018.

[35] Jonathan C.W. Brooks, Olivia K. Faull, Kyle T.S. Pattinson, and Mark Jenkinson. Physiological noise in brainstem fMRI. *Frontiers in Human Neuroscience*, 7(OCT):1–13, 2013.

[36] Rossitza Draganova, Viktor Pfaffenrot, Katharina M. Steiner, Sophia L. Goricke, Naveen Elangovan, Dagmar Timmann, and Jurgen Konczak. Neurostructural changes and declining sensorimotor function due to cerebellar cortical degeneration. *Journal of Neurophysiology*, 125(5):1735–1745, 2021.

[37] R. C. Oldfield. The assessment and analysis of handedness: The Edinburgh inventory. *Neuropsychologia*, 9(1):97–113, 1971.

[38] A. F. Fotenos, A. Z. Snyder, L. E. Girton, J. C. Morris, and R. L. Buckner. Normative estimates of cross-sectional and longitudinal brain volume decline in aging and AD. *Neurology*, 2005.

[39] Yulin Ge, Robert I. Grossman, James S. Babb, Marcie L. Rabin, Lois J. Mannon, and Dennis L. Kolson. Age-related total gray matter and white matter changes in normal adult brain. Part I: Volumetric MR imaging analysis. *American Journal of Neuroradiology*, 2002.

[40] Kazunori Sato, Yasuyuki Taki, Hiroshi Fukuda, and Ryuta Kawashima. Neuroanatomical database of normal Japanese brains. *Neural Networks*, 2003.

[41] Edith V. Sullivan, Margaret Rosenbloom, Kathleen L. Serventi, and Adolf Pfefferbaum. Effects of age and sex on volumes of the thalamus, pons, and cortex. *Neurobiology of Aging*, 2004.

[42] Yasuyuki Taki, Ryoi Goto, Alan Evans, Alex Zijdenbos, Peter Neelin, Jason Lerch, Kazunori Sato, Shuichi Ono, Shigeo Kinomura, Manabu Nakagawa, Motoaki Sugiura, Jobu Watanabe, Ryuta Kawashima, and Hiroshi Fukuda. Voxel-based morphometry of human brain with age and cerebrovascular risk factors. *Neurobiology of Aging*, 2004.

[43] Charles D. Smith, Himachandra Chebrolu, David R. Wekstein, Frederick A. Schmitt, and William R.

Markesbery. Age and gender effects on human brain anatomy: A voxel-based morphometric study in healthy elderly. *Neurobiology of Aging*, 2007.

[44] Hervé Lemaître, Fabrice Crivello, Blandine Grassiot, Annick Alpérovitch, Christophe Tzourio, and Bernard Mazoyer. Age- and sex-related effects on the neuroanatomy of healthy elderly. *NeuroImage*, 2005.

[45] Alan C. Evans, Andrew L. Janke, D. Louis Collins, and Sylvain Baillet. Brain templates and atlases. *NeuroImage*, 62(2):911–922, 2012.

[46] JD Schmahmann, Julien Doyon, AW Toga, M Petrides, and AC Evns. *MRI atlas of the human cerebellum*. 2000.

[47] Gholamreza Salimi-Khorshidi, Gwenaëlle Douaud, Christian F. Beckmann, Matthew F. Glasser, Ludovica Griffanti, and Stephen M. Smith. Automatic denoising of functional MRI data: Combining independent component analysis and hierarchical fusion of classifiers. *NeuroImage*, 90:449–468, 2014.

[48] D. M. Clower, J. M. Hoffman, J. R. Votaw, T. L. Faber, R. P. Woods, and G. E. Alexander. Role of posterior parietal cortex in the recalibration of visually guided reaching. *Nature*, 383(6601):618–621, 1996.

[49] John E. Schlerf, Joseph M. Galea, Amy J. Bastian, and Pablo A. Celnik. Dynamic modulation of cerebellar excitability for abrupt, but not gradual, visuomotor adaptation. *Journal of Neuroscience*, 32(34):11610–11617, 2012.

[50] Gowri Jayaram, Joseph M. Galea, Amy J. Bastian, and Pablo Celnik. Human locomotor adaptive learning is proportional to depression of cerebellar excitability. *Cerebral Cortex*, 21(8):1901–1909, 2011.

[51] Joaquin A. Anguera, Patricia A. Reuter-Lorenz, Daniel T. Willingham, and Rachael D. Seidler. Contributions of spatial working memory to visuomotor learning. *Journal of Cognitive Neuroscience*, 2010.

[52] Joaquin A. Anguera, Patricia A. Reuter-Lorenz, Daniel T. Willingham, and Rachael D. Seidler. Failure to engage spatial working memory contributes to age-related declines in visuomotor learning. *Journal of Cognitive Neuroscience*, 2011.

[53] Jordan A. Taylor, John W. Krakauer, and Richard B. Ivry. Explicit and implicit contributions to learning in a sensorimotor adaptation task. *Journal of Neuroscience*, 34(8):3023–3032, 2014.

[54] Caroline Nettekoven, Da Zhi, Ladan Shahshahani, Ana Luisa Pinho, Noam Saadon-grosman, and Jörn Diedrichsen. A hierarchical atlas of the human cerebellum for functional precision mapping. *bioRxiv*, pages 1–27, 2023.

[55] Alexandre Ivachtchenko, Yan Ivanenkov, and Mark Veselov. Preclinical evaluation of AVN-322, novel and highly selective 5-HT6 receptor antagonist, for the treatment of Alzheimer's disease. *Current Alzheimer Research*, 13(999):1–1, 2016.

[56] Pascal Fries. Rhythms for Cognition: Communication through Coherence, 2015.

[57] Christopher M. Lewis, Antonello Baldassarre, Giorgia Committeri, Gian Luca Romani, and Maurizio Corbetta. Learning sculpts the spontaneous activity of the resting human brain. *Proceedings of the National Academy of Sciences of the United States of America*, 106(41):17558–17563, 2009.

[58] Saber Sami, Edwin M. Robertson, and R. Chris Miall. The time course of task-specific memory consolidation effects in resting state networks. *Journal of Neuroscience*, 34(11):3982–3992, 2014.

[59] Neil B. Albert, Edwin M. Robertson, and R. Chris Miall. The Resting Human Brain and Motor Learning. *Current Biology*, 19(12):1023–1027, 2009.

[60] Caroline Nettekoven, Sinead Brady, William Clarke, Uzay E. Emir, Jacob Levenstein, Pierre Petitet, Muriel T N Panouilleres, Velicia Bachtiar, Jacinta O'Shea, Heidi Johansen-Berg, Ned Jenkinson, and Charlotte J. Stagg. GABA relates to functional connectivity changes and retention in visuomotor adaptation. *bioRxiv*, pages 1–29, 2020.

[61] Andreea C. Bostan, Richard P. Dum, and Peter L. Strick. Cerebellar networks with the cerebral cortex and basal ganglia. *Trends in Cognitive Sciences*, 17(5):241–254, 2013.

[62] M. Desmurget, C. M. Epstein, R. S. Turner, C. Prablanc, G. E. Alexander, and S. T. Grafton. Role of the posterior parietal cortex in updating reaching movements to a visual target. *Nature Neuroscience*, 2(6):563–567, 1999.

[63] Valeria Della-Maggiore and Anthony R. McIntosh. Time course of changes in brain activity and functional connectivity associated with long-term adaptation to a rotational transformation. *Journal*

*of Neurophysiology*, 93(4):2254–2262, 2005.

[64] J. Diedrichsen. Neural Correlates of Reach Errors. *Journal of Neuroscience*, 25(43):9919–9931, 2005.

[65] T. Schmitz-Hübsch, S. Tezenas Du Montcel, L. Baliko, J. Berciano, S. Boesch, C. Depondt, P. Giunti, C. Globas, J. Infante, J. S. Kang, B. Kremer, C. Mariotti, B. Melegh, M. Pandolfo, M. Rakowicz, P. Ribai, R. Rola, L. Schöls, S. Szymanski, B. P. Van De Warrenburg, A. Dürr, T. Klockgether, and Roberto Fancellu. Scale for the assessment and rating of ataxia: Development of a new clinical scale. *Neurology*, 2006.

[66] Mark Jenkinson, Christian F Beckmann, Timothy E J Behrens, Mark W Woolrich, and Stephen M Smith. Review FSL. *NeuroImage*, 62:782–790, 2012.

[67] Brian B. Avants, Paul Yushkevich, John Pluta, David Minkoff, Marc Korczykowski, John Detre, and James C. Gee. The optimal template effect in hippocampus studies of diseased populations. *NeuroImage*, 49(3):2457–2466, 2010.

[68] Paul A. Yushkevich, Joseph Piven, Heather Cody Hazlett, Rachel Gimpel Smith, Sean Ho, James C. Gee, and Guido Gerig. User-guided 3D active contour segmentation of anatomical structures: Significantly improved efficiency and reliability. *NeuroImage*, 2006.

[69] Evan S. Lutkenhoff, Matthew Rosenberg, Jeffrey Chiang, Kunyu Zhang, John D. Pickard, Adrian M. Owen, and Martin M. Monti. Optimized brain extraction for pathological brains (optiBET). *PLoS ONE*, 2014.

[70] Paul T. Fillmore, Michelle C. Phillips-Meek, and John E. Richards. Age-specific MRI brain and head templates for healthy adults from 20 through 89 years of age. *Frontiers in Aging Neuroscience*, 7(MAR):1–14, 2015.

[71] Jörn Diedrichsen, Joshua H. Balsters, Jonathan Flavell, Emma Cussans, and Narender Ramnani. A probabilistic MR atlas of the human cerebellum. *NeuroImage*, 46(1):39–46, 2009.

[72] Fidel Alfaro-Almagro, Mark Jenkinson, Neal K. Bangerter, Jesper L.R. Andersson, Ludovica Griffanti, Gwenaëlle Douaud, Stamatios N. Sotiropoulos, Saad Jbabdi, Moises Hernandez-Fernandez, Emmanuel Vallee, Diego Vidaurre, Matthew Webster, Paul McCarthy, Christopher Rorden, Alessandro Daducci, Daniel C. Alexander, Hui Zhang, Iulius Dragonu, Paul M. Matthews, Karla L. Miller, and Stephen M. Smith. Image processing and Quality Control for the first 10,000 brain imaging datasets from UK Biobank. *NeuroImage*, 166(October 2017):400–424, 2018.

[73] J. K. Smith, A. Londono, M. Castillo, and L. Kwock. Proton magnetic resonance spectroscopy of brain-stem lesions. *Neuroradiology*, 44(10):825–829, 2002.

[74] Mark Jenkinson, Peter Bannister, Michael Brady, and Stephen Smith. Improved Optimization for the Robust and Accurate Linear Registration and Motion Correction of Brain Images. *NeuroImage*, 17(2):825–841, 2002.

[75] Mark Jenkinson and Stephen Smith. A global optimisation method for robust affine registration of brain images. *Medical Image Analysis*, 5(2):143–156, 2001.

[76] Douglas N Greve and Bruce Fischl. Accurate and robust brain image alignment using boundary-based registration, 2009.

[77] Ludovica Griffanti, Gholamreza Salimi-Khorshidi, Christian F. Beckmann, Edward J. Auerbach, Gwenaëlle Douaud, Claire E. Sexton, Eniko Zsoldos, Klaus P. Ebmeier, Nicola Filippini, Clare E. Mackay, Steen Moeller, Junqian Xu, Essa Yacoub, Giuseppe Baselli, Kamil Ugurbil, Karla L. Miller, and Stephen M. Smith. ICA-based artefact removal and accelerated fMRI acquisition for improved resting state network imaging. *NeuroImage*, 95:232–247, 2014.

[78] Luke Baxter, Sean Fitzgibbon, Fiona Moultrie, Sezgi Goksan, Mark Jenkinson, Stephen Smith, Jesper Andersson, Eugene Duff, and Rebeccah Slater. Optimising neonatal fMRI data analysis: Design and validation of an extended dHCP preprocessing pipeline to characterise noxious-evoked brain activity in infants. *NeuroImage*, 186(October 2018):286–300, 2019.

[79] Piergiorgio Salvan, Thomas Wassenaar, Catherine Wheatley, Nicholas Beale, Michiel Cottaar, Daniel Papp, Matteo Bastiani, Sean Fitzgibbon, Euguene Duff, Jesper Andersson, Anderson M. Winkler, Gwenaëlle Douaud, Thomas E. Nichols, Stephen Smith, Helen Dawes, and Heidi Johansen-Berg. Multimodal imaging brain markers in early adolescence are linked with a physically active lifestyle. *Journal of Neuroscience*, 41(5):1092–1104, 2021.

[80] Christiane A. Weinrich, John Stuart Brittain, Magdalena Nowak, Reza Salimi-Khorshidi, Peter Brown, and Charlotte J. Stagg. Modulation of Long-Range Connectivity Patterns via Frequency-Specific

Stimulation of Human Cortex. *Current Biology*, 27(19):3061–3068.e3, 2017.

[81] Valentina Tomassini, Saad Jbabdi, Johannes C. Klein, Timothy E.J. Behrens, Carlo Pozzilli, Paul M. Matthews, Matthew F.S. Rushworth, and Heidi Johansen-Berg. Diffusion-weighted imaging tractography-based parcellation of the human lateral premotor cortex identifies dorsal and ventral subregions with anatomical and functional specializations. *Journal of Neuroscience*, 2007.

[82] Katrin Amunts, Hartmut Mohlberg, Sebastian Bludau, and Karl Zilles. Julich-Brain: A 3D probabilistic atlas of the human brain's cytoarchitecture. *Science*, 2020.

[83] Jérôme Sallet, Rogier B. Mars, Maryann P. Noonan, Franz Xaver Neubert, Saad Jbabdi, Jill X. O'Reilly, Nicola Filippini, Adam G. Thomas, and Matthew F. Rushworth. The organization of dorsal frontal cortex in humans and macaques. *Journal of Neuroscience*, 33(30):12255–12274, 2013.

[84] Ladan Shahshahani, Maedbh King, Caroline Nettekoven, Richard Ivry, and Jörn Diedrichsen. Selective recruitment : Evidence for task-dependent gating of inputs to the cerebellum. *bioRxiv*, pages 1–17, 2023.

[85] Franziska Hoche, Xavier Guell, Mark G. Vangel, Janet C. Sherman, and Jeremy D. Schmahmann. The cerebellar cognitive affective/Schmahmann syndrome scale. *Brain*, 141(1):248–270, 2018.

[86] R Development Core Team 3.0.1. A Language and Environment for Statistical Computing, 2013.

[87] Pauli Virtanen, Ralf Gommers, Travis E. Oliphant, Matt Haberland, Tyler Reddy, David Cournapeau, Evgeni Burovski, Pearu Peterson, Warren Weckesser, Jonathan Bright, Stéfan J. van der Walt, Matthew Brett, Joshua Wilson, K. Jarrod Millman, Nikolay Mayorov, Andrew R.J. Nelson, Eric Jones, Robert Kern, Eric Larson, C. J. Carey, İlhan Polat, Yu Feng, Eric W. Moore, Jake VanderPlas, Denis Laxalde, Josef Perktold, Robert Cimrman, Ian Henriksen, E. A. Quintero, Charles R. Harris, Anne M. Archibald, Antônio H. Ribeiro, Fabian Pedregosa, Paul van Mulbregt, Aditya Vijaykumar, Alessandro Pietro Bardelli, Alex Rothberg, Andreas Hilboll, Andreas Kloeckner, Anthony Scopatz, Antony Lee, Ariel Rokem, C. Nathan Woods, Chad Fulton, Charles Masson, Christian Häggström, Clark Fitzgerald, David A. Nicholson, David R. Hagen, Dmitrii V. Pasechnik, Emanuele Olivetti, Eric Martin, Eric Wieser, Fabrice Silva, Felix Lenders, Florian Wilhelm, G. Young, Gavin A. Price, Gert Ludwig Ingold, Gregory E. Allen, Gregory R. Lee, Hervé Audren, Irvin Probst, Jörg P. Dietrich, Jacob Silterra, James T. Webber, Janko Slavič, Joel Nothman, Johannes Buchner, Johannes Kulick, Johannes L. Schönberger, José Vinícius de Miranda Cardoso, Joscha Reimer, Joseph Harrington, Juan Luis Cano Rodríguez, Juan Nunez-Iglesias, Justin Kuczynski, Kevin Tritz, Martin Thoma, Matthew Newville, Matthias Kümmerer, Maximilian Bolingbroke, Michael Tartre, Mikhail Pak, Nathaniel J. Smith, Nikolai Nowaczyk, Nikolay Shebanov, Oleksandr Pavlyk, Per A. Brodtkorb, Perry Lee, Robert T. McGibbon, Roman Feldbauer, Sam Lewis, Sam Tygier, Scott Sievert, Sebastiano Vigna, Stefan Peterson, Surhud More, Tadeusz Pudlik, Takuya Oshima, Thomas J. Pingel, Thomas P. Robitaille, Thomas Spura, Thouis R. Jones, Tim Cera, Tim Leslie, Tiziano Zito, Tom Krauss, Utkarsh Upadhyay, Yaroslav O. Halchenko, and Yoshiki Vázquez-Baeza. SciPy 1.0: fundamental algorithms for scientific computing in Python. *Nature Methods*, 2020.

[88] Alexandra Kuznetsova, Per B. Brockhoff, and Rune H.B. Christensen. lmerTest Package: Tests in Linear Mixed Effects Models. *Journal of Statistical Software*, 2017.

[89] Yoav Benjamini and Yosef Hochberg. Controlling the False Discovery Rate: A Practical and Powerful Approach to Multiple Testing. *Journal of the Royal Statistical Society: Series B (Methodological)*, 1995.

[90] Yoav Benjamini and Daniel Yekutieli. The control of the false discovery rate in multiple testing under dependency. *Annals of Statistics*, 2001.

## 5 DATA AVAILABILITY

The study-specific template is publicly available at `https://github.com/carobellum/DegenerationControlTemplate`.
The template validation data is publicly available at `https://github.com/carobellum/DegenerationConnectivity/data` along with the extracted timeseries data supporting the connectivity findings of this study. Due to data privacy restrictions, the raw MRI data has not been openly released, but can be made available upon request to the corresponding author.

## 6 CODE AVAILABILITY

The code for generating and validating the template, analyzing the functional connectivity data and for recreating the results and figures in this paper is publicly available as the GitHub repository `https://github.com/carobellum/DegenerationConnectivity`.


## ACKNOWLEDGEMENTS

This study was funded by a research grant of the German Research Foundation awarded to J. K. and D. T. (DFG TI 239/14-1), and a research grant of the Bernd Fink Foundation awarded to J. K. and D. T.. We would like to acknowledge Jacob Levenstein for providing advice on template generation and Joern Diedrichsen for helpful discussions about template validation. Special thanks to Beate Brol for hand-correcting cerebellar masks and manually drawing cerebellar fissures.


## AUTHOR CONTRIBUTIONS

R.D., J.K. and D.T. designed the research; R.D., K.M.S., S.L.G. and A.D. performed the research; C.N. analyzed the data; C.N. wrote the first draft of the paper, C.N., R.D., J.K. and D.T. revised the paper.

## COMPETING INTERESTS

The authors declare no competing interests.

# 7 SUPPLEMENTARY MATERIALS

| | Age | | Sex | | Group | | Condition | | | | Timepoint | |
|---|---|---|---|---|---|---|---|---|---|---|---|---|
| Sample | Mean | Std | M | F | Patient | Control | V | NV | V+F | NV+F | Pre | Post |
| Validation | 53.97 | 11.85 | 22 | 18 | 20 | 20 | 10 | 10 | 10 | 10 | 40 | 0 |
| Generation | 57.15 | 9.96 | 23 | 17 | 20 | 20 | 10 | 10 | 10 | 10 | 21 | 19 |

**Table 1. Template generation and validation sample demographics.** Demographic data for scans included into the study-specific template (generation sample) and held out from the template (validation sample). Generation scans were balanced across groups and conditions and approximately balanced across age, sex, and timepoint. Conditions are vision (V), no vision (NV), vision with explicit feedback (V+F), and no vision with explicit feedback (NV+F).

| Sample | Fissure | Area | MNI template | SUIT template | DeCon template |
|---|---|---|---|---|---|
| Validation | Primary | Cerebellum | 3.80 (0.73) | 3.24 (0.74) | 2.26 (0.67) |
| | | Vermis | 3.22 (0.95) | 2.40 (0.74) | 0.96 (1.04) |
| | Intrabiventer | Cerebellum | 3.22 (0.51) | 2.71 (0.48) | 1.83 (0.40) |
| Generation | Primary | Cerebellum | 4.04 (1.36) | 3.41 (1.05) | 2.25 (0.71) |
| | | Vermis | 3.16 (1.16) | 2.37 (0.85) | 0.81 (0.32) |
| | Intrabiventer | Cerebellum | 3.51 (0.68) | 2.97 (0.70) | 2.06 (0.79) |

**Table 2. Fissure distances.** Average pairwise fissure distances fur subjects included into the study-specific template (generation sample) and held out from the template (validation sample). Distances are given as mean (standard deviation).

| | Sum Sq | Mean Sq | NumDF | DenDF | F value | Pr(>F) |
|---|---|---|---|---|---|---|
| group | 0.12 | 0.12 | 1 | 79.00 | 4.73 | 0.0326 |
| region_type | 8.48 | 4.24 | 2.00 | 158.00 | 162.55 | 0.0000 |
| group x region_type | 0.39 | 0.19 | 2.00 | 158.00 | 7.46 | 0.0008 |

**Table 3.** Linear mixed effects model for connectivity at baseline

| | Sum Sq | Mean Sq | NumDF | DenDF | F value | Pr(>F) |
|---|---|---|---|---|---|---|
| group | 0.13 | 0.13 | 1 | 78.76 | 5.03 | 0.0277 |
| session | 0.21 | 0.21 | 1 | 78.15 | 8.33 | 0.0050 |
| vision | 0.00 | 0.00 | 1 | 78.76 | 0.04 | 0.8509 |
| feedback | 0.03 | 0.03 | 1 | 78.76 | 1.15 | 0.2872 |
| group x session | 0.05 | 0.05 | 1 | 78.15 | 1.99 | 0.1624 |
| group x vision | 0.03 | 0.03 | 1 | 78.76 | 1.37 | 0.2461 |
| session x vision | 0.21 | 0.21 | 1 | 78.15 | 8.11 | 0.0056 |
| group x feedback | 0.00 | 0.00 | 1 | 78.76 | 0.05 | 0.8223 |
| session x feedback | 0.00 | 0.00 | 1 | 78.15 | 0.11 | 0.7447 |
| vision x feedback | 0.00 | 0.00 | 1 | 78.76 | 0.19 | 0.6666 |
| group x session x vision | 0.00 | 0.00 | 1 | 78.15 | 0.12 | 0.7306 |
| group x session x feedback | 0.03 | 0.03 | 1 | 78.15 | 1.24 | 0.2681 |
| group x vision x feedback | 0.01 | 0.01 | 1 | 78.76 | 0.39 | 0.5346 |
| session x vision x feedback | 0.07 | 0.07 | 1 | 78.15 | 2.79 | 0.0986 |
| group x session x vision x feedback | 0.04 | 0.04 | 1 | 78.15 | 1.53 | 0.2199 |

**Table 4.** Linear mixed effects model for connectivity between pmd-left and cereb-M3-right

| | Sum Sq | Mean Sq | NumDF | DenDF | F value | Pr(>F) |
|---|---|---|---|---|---|---|
| group | 0.19 | 0.19 | 1 | 78.82 | 7.47 | 0.0078 |
| session | 0.03 | 0.03 | 1 | 78.20 | 0.99 | 0.3227 |
| vision | 0.00 | 0.00 | 1 | 78.82 | 0.08 | 0.7778 |
| feedback | 0.08 | 0.08 | 1 | 78.82 | 3.08 | 0.0831 |
| group x session | 0.04 | 0.04 | 1 | 78.20 | 1.63 | 0.2055 |
| group x vision | 0.02 | 0.02 | 1 | 78.82 | 0.79 | 0.3754 |
| session x vision | 0.06 | 0.06 | 1 | 78.20 | 2.34 | 0.1299 |
| group x feedback | 0.01 | 0.01 | 1 | 78.82 | 0.20 | 0.6546 |
| session x feedback | 0.07 | 0.07 | 1 | 78.20 | 2.61 | 0.1101 |
| vision x feedback | 0.00 | 0.00 | 1 | 78.82 | 0.00 | 0.9730 |
| group x session x vision | 0.15 | 0.15 | 1 | 78.20 | 5.75 | 0.0189 |
| group x session x feedback | 0.02 | 0.02 | 1 | 78.20 | 0.92 | 0.3398 |
| group x vision x feedback | 0.00 | 0.00 | 1 | 78.82 | 0.00 | 0.9911 |
| session x vision x feedback | 0.09 | 0.09 | 1 | 78.20 | 3.54 | 0.0637 |
| group x session x vision x feedback | 0.06 | 0.06 | 1 | 78.20 | 2.50 | 0.1178 |

**Table 5.** Linear mixed effects model for connectivity between pmd-right and cereb-M3-left

| | Sum Sq | Mean Sq | NumDF | DenDF | F value | Pr(>F) |
|---|---|---|---|---|---|---|
| group | 0.12 | 0.12 | 1 | 78.96 | 4.85 | 0.0305 |
| session | 0.12 | 0.12 | 1 | 78.30 | 4.95 | 0.0290 |
| vision | 0.00 | 0.00 | 1 | 78.96 | 0.06 | 0.8042 |
| group x session | 0.00 | 0.00 | 1 | 78.30 | 0.16 | 0.6935 |
| group x vision | 0.01 | 0.01 | 1 | 78.96 | 0.49 | 0.4867 |
| session x vision | 0.18 | 0.18 | 1 | 78.30 | 7.21 | 0.0088 |
| group x session x vision | 0.01 | 0.01 | 1 | 78.30 | 0.49 | 0.4874 |

**Table 6.** Linear mixed effects model for connectivity between ppc-left and cereb-M3-right

| | Sum Sq | Mean Sq | NumDF | DenDF | F value | Pr(>F) |
|---|---|---|---|---|---|---|
| group | 0.31 | 0.31 | 1 | 79.23 | 9.11 | 0.0034 |
| session | 0.01 | 0.01 | 1 | 78.70 | 0.26 | 0.6110 |
| vision | 0.00 | 0.00 | 1 | 79.23 | 0.01 | 0.9375 |
| group x session | 0.02 | 0.02 | 1 | 78.70 | 0.73 | 0.3965 |
| group x vision | 0.02 | 0.02 | 1 | 79.23 | 0.63 | 0.4304 |
| session x vision | 0.20 | 0.20 | 1 | 78.70 | 5.94 | 0.0171 |
| group x session x vision | 0.04 | 0.04 | 1 | 78.70 | 1.05 | 0.3092 |

**Table 7.** Linear mixed effects model for connectivity between ppc-right and cereb-M3-left

| | Sum Sq | Mean Sq | NumDF | DenDF | F value | Pr(>F) |
|---|---|---|---|---|---|---|
| group | 0.15 | 0.15 | 1.00 | 78.29 | 8.69 | 0.0042 |
| session | 0.08 | 0.08 | 1.00 | 77.86 | 4.64 | 0.0343 |
| vision | 0.01 | 0.01 | 1.00 | 78.29 | 0.34 | 0.5608 |
| feedback | 0.04 | 0.04 | 1.00 | 78.29 | 2.11 | 0.1503 |
| group:session | 0.00 | 0.00 | 1.00 | 77.86 | 0.03 | 0.8624 |
| group:vision | 0.00 | 0.00 | 1.00 | 78.29 | 0.20 | 0.6572 |
| session:vision | 0.06 | 0.06 | 1.00 | 77.86 | 3.34 | 0.0716 |
| group:feedback | 0.04 | 0.04 | 1.00 | 78.29 | 2.09 | 0.1527 |
| session:feedback | 0.01 | 0.01 | 1.00 | 77.86 | 0.41 | 0.5254 |
| vision:feedback | 0.01 | 0.01 | 1.00 | 78.29 | 0.34 | 0.5590 |
| group:session:vision | 0.03 | 0.03 | 1.00 | 77.86 | 1.54 | 0.2181 |
| group:session:feedback | 0.01 | 0.01 | 1.00 | 77.86 | 0.77 | 0.3826 |
| group:vision:feedback | 0.00 | 0.00 | 1.00 | 78.29 | 0.14 | 0.7099 |
| session:vision:feedback | 0.00 | 0.00 | 1.00 | 77.86 | 0.14 | 0.7129 |
| group:session:vision:feedback | 0.00 | 0.00 | 1.00 | 77.86 | 0.00 | 0.9766 |

**Table 8.** Linear mixed effects model for connectivity between m1-hand-left and cereb-M3-right

| | Sum Sq | Mean Sq | NumDF | DenDF | F value | Pr(>F) |
|---|---|---|---|---|---|---|
| group | 0.11 | 0.11 | 1.00 | 78.84 | 5.56 | 0.0208 |
| session | 0.08 | 0.08 | 1.00 | 78.46 | 3.78 | 0.0555 |
| vision | 0.00 | 0.00 | 1.00 | 78.84 | 0.11 | 0.7405 |
| feedback | 0.04 | 0.04 | 1.00 | 78.84 | 2.24 | 0.1387 |
| group:session | 0.05 | 0.05 | 1.00 | 78.46 | 2.34 | 0.1301 |
| group:vision | 0.00 | 0.00 | 1.00 | 78.84 | 0.03 | 0.8564 |
| session:vision | 0.07 | 0.07 | 1.00 | 78.46 | 3.39 | 0.0693 |
| group:feedback | 0.01 | 0.01 | 1.00 | 78.84 | 0.47 | 0.4966 |
| session:feedback | 0.08 | 0.08 | 1.00 | 78.46 | 3.90 | 0.0517 |
| vision:feedback | 0.00 | 0.00 | 1.00 | 78.84 | 0.12 | 0.7328 |
| group:session:vision | 0.02 | 0.02 | 1.00 | 78.46 | 0.89 | 0.3477 |
| group:session:feedback | 0.06 | 0.06 | 1.00 | 78.46 | 3.23 | 0.0764 |
| group:vision:feedback | 0.00 | 0.00 | 1.00 | 78.84 | 0.03 | 0.8694 |
| session:vision:feedback | 0.00 | 0.00 | 1.00 | 78.46 | 0.20 | 0.6582 |
| group:session:vision:feedback | 0.01 | 0.01 | 1.00 | 78.46 | 0.72 | 0.3998 |

**Table 9.** Linear mixed effects model for connectivity between m1-hand-right and cereb-M3-left

| | Sum Sq | Mean Sq | NumDF | DenDF | F value | Pr(>F) |
|---|---|---|---|---|---|---|
| group | 0.03 | 0.03 | 1 | 79.30 | 0.97 | 0.3286 |
| session | 0.06 | 0.06 | 1 | 78.83 | 1.69 | 0.1980 |
| feedback | 0.07 | 0.07 | 1 | 79.30 | 2.11 | 0.1503 |
| vision | 0.01 | 0.01 | 1 | 79.30 | 0.16 | 0.6868 |
| group x session | 0.01 | 0.01 | 1 | 78.83 | 0.25 | 0.6191 |
| group x feedback | 0.11 | 0.11 | 1 | 79.30 | 3.23 | 0.0759 |
| session x feedback | 0.01 | 0.01 | 1 | 78.83 | 0.34 | 0.5627 |
| group x vision | 0.00 | 0.00 | 1 | 79.30 | 0.00 | 0.9906 |
| session x vision | 0.03 | 0.03 | 1 | 78.83 | 0.87 | 0.3535 |
| feedback x vision | 0.01 | 0.01 | 1 | 79.30 | 0.21 | 0.6491 |
| group x session x feedback | 0.18 | 0.18 | 1 | 78.83 | 5.09 | 0.0269 |
| group x session x vision | 0.00 | 0.00 | 1 | 78.83 | 0.02 | 0.8943 |
| group x feedback x vision | 0.00 | 0.00 | 1 | 79.30 | 0.05 | 0.8245 |
| session x feedback x vision | 0.08 | 0.08 | 1 | 78.83 | 2.31 | 0.1322 |
| group x session x feedback x vision | 0.00 | 0.00 | 1 | 78.83 | 0.09 | 0.7601 |

**Table 10.** Linear mixed effects model for connectivity between dlpfc-right and cereb-D2-right